



Gas-sensing properties of ITO materials with different morphologies prepared by sputtering

Yuantao Zhang^{1,2} · Qiang Li^{1,2} · Zhenhuan Tian² · Peng Hu² · Xiao Qin² · Feng Yun^{1,2}Received: 7 September 2019 / Accepted: 15 January 2020 / Published online: 23 January 2020
© Springer Nature Switzerland AG 2020

Abstract

Indium tin oxide (ITO) materials with different morphologies have been fabricated via sputtering technology by adjusting the oxygen flow rate and RF-power. The repeatable and controllable growth conditions of different ITO materials have been achieved. The gas sensors with different ITO materials were fabricated on ceramic tube directly, which have the characteristics of low cost and simple preparation process. Through our analysis, the nanowires have larger specific surface area, more oxygen vacancies and an oriented electron transport channel. The sensor made by nanowires was the best one, and the value of sensitivity run up to 235.6 at the ethanol gas concentration of 400 ppm under 250 °C. The gas sensing properties of the whole ITO material system to ethanol gas were studied. The difference of gas sensing properties is explained by calculating the surface adsorption energy of ITO materials with different morphologies based on first-principle calculation method. These results provide guidance for the application of ITO materials in the field of gas sensors.

Keywords Gas sensor · ITO nanowires · First principle · Sputtering technology

1 Introduction

Indium tin oxide (ITO) is an *n*-type semiconductor with a wide band-gap of 3.5–4.06 eV [1], which has received a considerable attention due to its multifunctional properties and wide applications in electronics, optoelectronics and sensors [2–4]. ITO and ITO-based nanomaterials are potential candidates for the fabrication of electrochemical device, biochemical device and gas sensor [5–9]. Recently, developments in the field of sensors based on multifunctional ITO nanomaterials have led to the fabrication of highly sensitive and selective sensors. There are many reports on gas sensitive devices fabricated by ITO materials. A. Ayeshamariam, et al. studied the gas sensing properties of ITO nanoparticles fabricated by combustion synthesis [10]. The sensitivity was 14.436 at the ethanol gas

concentration of 100 ppm. Yao et al. [11] reported the high sensitivity of ITO nanorods for NO₂ prepared by oblique angle deposition. The detection limit reached to 50 ppb with a response time of 20 min. Afshar et al. [12] fabricated the gas sensor using ITO nanowires via laser writing and subsequent etching. The sensors were exposed to NO₂ in synthetic air with concentrations from 1 to 50 ppm showing a significant change in resistance. Zhou et al. [13] designed a type of high-surface ITO nanotubes by single-nozzle electro spinning technique to research the gas sensing properties. The sensors based on nanotubes exhibited its maximum response at low temperature of 160 °C, and could quick respond to 100 ppm formaldehyde even at temperature less than 100 °C. However, all these methods are used to study single material independently

✉ Qiang Li, liqiang2014@mail.xjtu.edu.cn; ✉ Feng Yun, fyun2010@mail.xjtu.edu.cn | ¹Key Laboratory of Physical Electronics and Devices for Ministry of Education and Shaanxi Provincial Key Laboratory of Photonics and Information Technology, Xi'an Jiaotong University, Xi'an 710049, Shaanxi, People's Republic of China. ²School of Electronic and Information Engineering, Xi'an Jiaotong University, Xi'an 710049, Shaanxi, People's Republic of China.



and there is no systematic study on the gas sensing properties of the whole material system.

ITO nanostructures have higher surface-volume ratio, result in a higher gas sensitivity compared with bulk materials. Many methods have been tried to obtain ITO nanostructures, such as sputtering, thermal evaporation, and electron beam evaporation [14–16]. Among all of these methods, magnetron sputtering is the best choice, because of the faster deposition rate, better film quality, and the more stable repeatability [17, 18].

In our previous work, ITO nanowires have been fabricated through self-catalytic vapor–liquid–solid (VLS) mechanism by sputtering, which showed good conductivity and good transmittance [19]. In this paper, ITO materials with different morphologies have been fabricated by adjusting the oxygen flow rate and RF-power. The repeatable and controllable growth conditions of different ITO materials have been obtained. Then the gas sensors based on different ITO materials were fabricated with low cost and simple preparation process. The gas-sensing properties were tested, and the effect of morphology on sensing performance was also analyzed. For ITO-nanowire gas sensor, the effect of temperature and density of ITO nanowires on sensing performance was investigated. Finally, the surface adsorption energy of ITO materials with different morphologies was calculated by the first-principle calculation method.

2 Experiment

2.1 The preparation of ITO materials

ITO materials were deposited on silicon and ceramic tube by RF-magnetron sputtering. The ITO target is composed of 90 wt% In_2O_3 and 10 wt% SnO_2 . The deposition process was carried out under the background pressure of 1.5×10^{-4} Pa and the temperature of 500 °C. The working pressure is 1 Pa and the argon flow rate is 25 sccm. The sputtering power and the oxygen flow rate were adjusted in order to obtain different ITO morphologies. Two different RF-powers (200 W, 250 W) and three different oxygen flow rates (0, 0.1 sccm, and 0.2 sccm) were used. The sputtering time is 20 min and then the chamber was cooled down to room temperature naturally.

2.2 The preparation of gas sensor

Figure 1 was a real photo of the fabricated sensor. The ceramic tube in the Fig. 1a was used as substrate for the preparation of gas sensor. Before deposition, the silicon (Si) and ceramic tube were ultrasonically cleaned in alcohol to remove organic contaminant on the surface. After

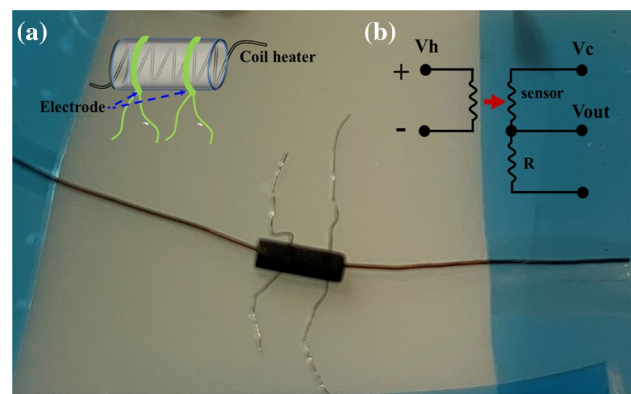


Fig. 1 The fabricated sensor **a** ceramic tube used in gas sensor, **b** test principle diagram

the sputtering, a coil heater was placed inside the ceramic tube and the device was connected to the test instrument by gold wire. The pressure of testing chamber was maintained at atmospheric condition. The gas-sensing properties of the devices were tested on a WS-30A gas sensor system (Wei-Sheng Electronics Co. Ltd., Zhengzhou, China) under a relative humidity less than 30%RH at room temperature. Figure 1b shows the test principle of the test instrument. The change of device resistance could lead to the change of output voltage (V-out). The gas sensing properties of ITO materials to ethanol gas could be investigated at different temperatures.

In order to characterize material properties, the morphologies of ITO materials were analyzed by scanning electron microscopy (SEM), and the binding energy of materials were analyzed by X-ray photoelectron spectroscopy (XPS).

3 Results and discussion

3.1 Different morphologies of ITO materials

Different morphologies of ITO materials were fabricated by adjusting RF-power and the oxygen flow rate. The SEM images were shown in Fig. 2. The process parameters for power and oxygen flow rate could be found in Table 1. The chamber temperature and the argon flow rate were always maintained at 500 °C and 25 sccm, respectively.

Oxygen is the main factor affecting the morphologies of ITO materials. The ITO materials were fabricated with different oxygen flow rates of 0, 0.1 and 0.2 sccm. The growth of nanorods and nanowires only happened without oxygen (Fig. 2). The ITO nanostructures (nanowires or nanorods) usually are prepared through VLS mechanism, the alloy droplets during nucleation process are extremely important for the growth of nanostructures. In sputtering

Fig. 2 SEM images of ITO materials with different morphologies by sputtering

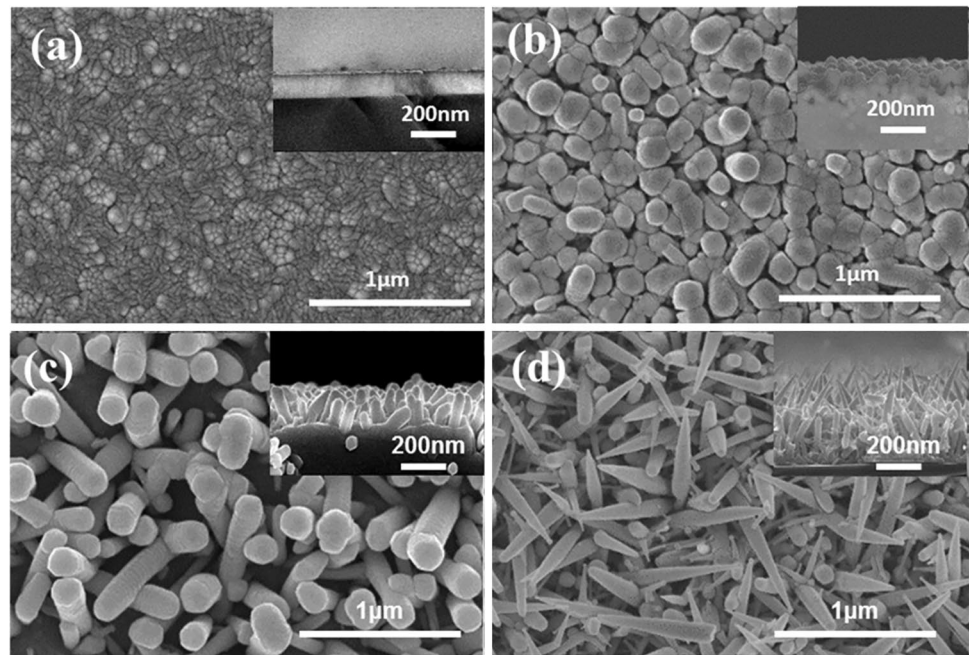


Table 1 Process parameters of sputtering for different ITO morphologies

Sample	RF-power (W)	Oxygen flow rate (sccm)
a	250	0.2
b	250	0.1
c	200	0
d	250	0

process, In and Sn atoms could be sputtered out of the target, and some of them would combine to form In-Sn alloy droplets. The nanowires and nanorods would grow up based on these alloy particles under anoxic condition. With increasing of the oxygen content, In_2O_3 and SnO_2 molecules produced. When the oxygen was not sufficient (under the condition of oxygen flow rate of 0.1 sccm), the large ITO-particles would be formed. When the oxygen was adequate ($\text{O}_2 = 0.2$ sccm), the ITO film would be obtained. In our previous report [19], we found that the growth of ITO nanostructures only happened when the sputtering power is larger than 200 W. In this work, the power was selected with 200 W and 250 W. Generally speaking, the growth rate of film is proportional to the sputtering power [20]. Under the power of 200 W, the molecules reunited together and attached the substrate. The nanorods began to grow based on these large droplets. When the power is up to 250 W, In-Sn droplets were attached on the substrate firstly and the molecules entered the alloy droplets in a short time to reach the super-saturation state. And

then, the nanowires begin to grow via In-Sn droplets as catalysts.

The different densities of ITO nanowires have been prepared by controlling the growth time (5 min, 15 min, and 25 min). The different densities of ITO nanowires were shown in Fig. 3. The length and density of nanowires increase with increasing growth time.

So, the optimized parameters for the preparation of nanowires are the RF-power of 250 W without oxygen, and the sputtering time is more than 15 min.

3.2 XPS characterizations

The Fig. 4 shows the XPS results for different morphologies of ITO materials. The element atomic percentages of In, Sn and O were listed in Table 2. The difference of atomic percentage among the film, particle and nanorod is small. The conductivity of ITO materials can be influenced by the oxygen vacancies inside the materials, so the $\text{O}1\text{ s}$ curves were separated from the XPS results. As shown in Fig. 5, the peak value of curve at 530 eV ~ 531 eV stands for the absorbed oxygen (O^{2-} , O^-) on the surface, and the peak of ~ 529 eV represents the lattice oxygen inside the materials. In order to characterize the difference between different materials, the atomic percentage was calculated by curvilinear integral and the results were summarized in Table 3.

Compared with other materials, nanowires have the least percentage of lattice oxygen, which means that the oxygen vacancies inside the nanowires are the most. More absorbed oxygen vacancies could be created on the

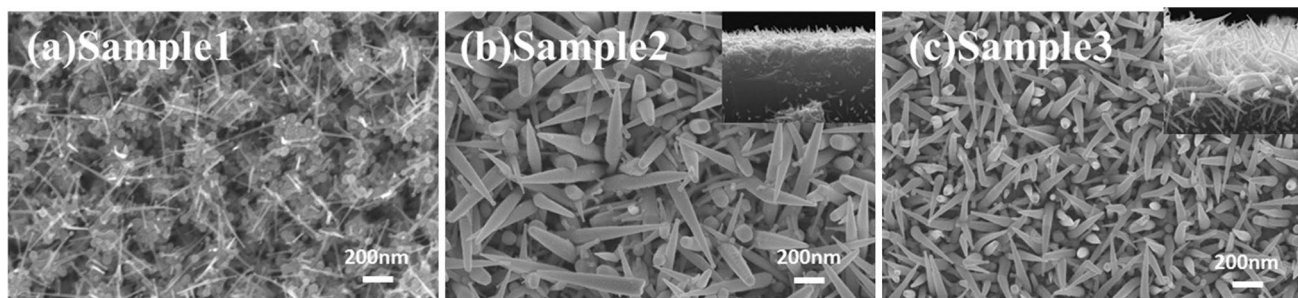


Fig. 3 SEM images of ITO nanowires with different densities at growth time **a** 5 min; **b** 15 min; **c** 25 min

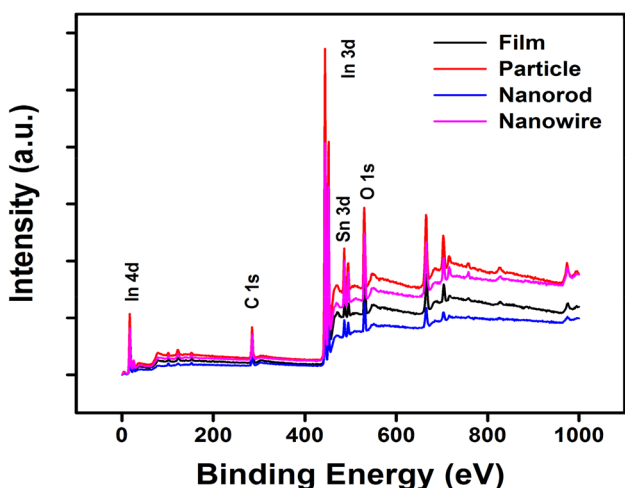


Fig. 4 XPS spectra of ITO materials with different morphologies

Table 2 Element atomic percentages of ITO materials with different morphologies

	Film	Particle	Nanorod	Nanowire
In	28.91	28.64	24.03	25.25
O	68.04	67.58	71.55	69.95
Sn	3.06	3.77	4.43	4.8

surface of nanowires, so the gas sensing properties were improved.

3.3 Gas sensing properties

Gas sensors with different morphologies of ITO materials have been prepared on ceramic tube directly. The sensing properties to ethanol gas were tested at different conditions. In order to eliminate the effect of materials' mass on the devices, the response (RS) was proposed, and defined as $RS = R_{air} / (m * R_{gas})$, where R_{air} and R_{gas} are the resistance values measured in the air and reducing-gas ambiances,

respectively. The m is the mass of the coated sensing materials.

Firstly, the gas sensing properties with different morphologies (film, particle, nanorod, and nanowire) were investigated under the conditions of the ethanol gas concentration of 400 ppm and the temperature of 250 °C. The gas sensitivities, response and recovery time of sensors with different morphologies were shown in Fig. 6. The RS for the ITO-film, -particle, -nanorod and -nanowire were 55.6, 62.4, 73.3 and 79.6, respectively. The response/recovery time is 17 s/32 s, 14 s/28 s, 12 s/23 s and 9 s/15 s, respectively. The results show that the sensitivity increases and response/recovery time decreases when the ITO materials tend to be finer nanostructures. Due to the reduction in dimension of materials, the surface-to-volume ratio of materials increases, leading to more sufficient reaction between the gas and materials. This is more favorable for desorption of materials and absorption of the reaction gas. At the same time, the reduction in dimensions limits the movement direction of carriers, so the mobility of carriers along the specific direction is high. So, the reduction in dimensions of ITO materials could be used to improve the gas sensing properties.

Moreover, the influence of temperature on the sensing performance was investigated. In Fig. 7, the line shows the sensitivity of sensor with ITO-nanowires at different operating temperatures. At the temperatures of 100 °C, 150 °C, 200 °C, 250 °C and 300 °C, the RS were 55.0, 59.2, 68.0, 77.2, and 83.7, respectively. The RS improved with temperature increasing. This phenomenon can be explained by the metal oxide semiconductor sensing mechanism [21, 22].

Under the air ambient, the oxygen molecules were absorbed on the surface of the sensor materials. The absorbed oxygen molecules could capture electrons from the ITO conduction band and form O_2^- , O^- , O^{2-} , and then a depletion layer on the surface was formed, leading to a high resistance of sensor. Once the sensors were placed in the ethanol gas, the reaction between the gas and absorbed oxygen ion could release the electron back to conduction band, resulting in the resistance of sensors

Fig. 5 The spectrum of O 1s, **a** film, **b** particle, **c** nanorod, **d** nanowire

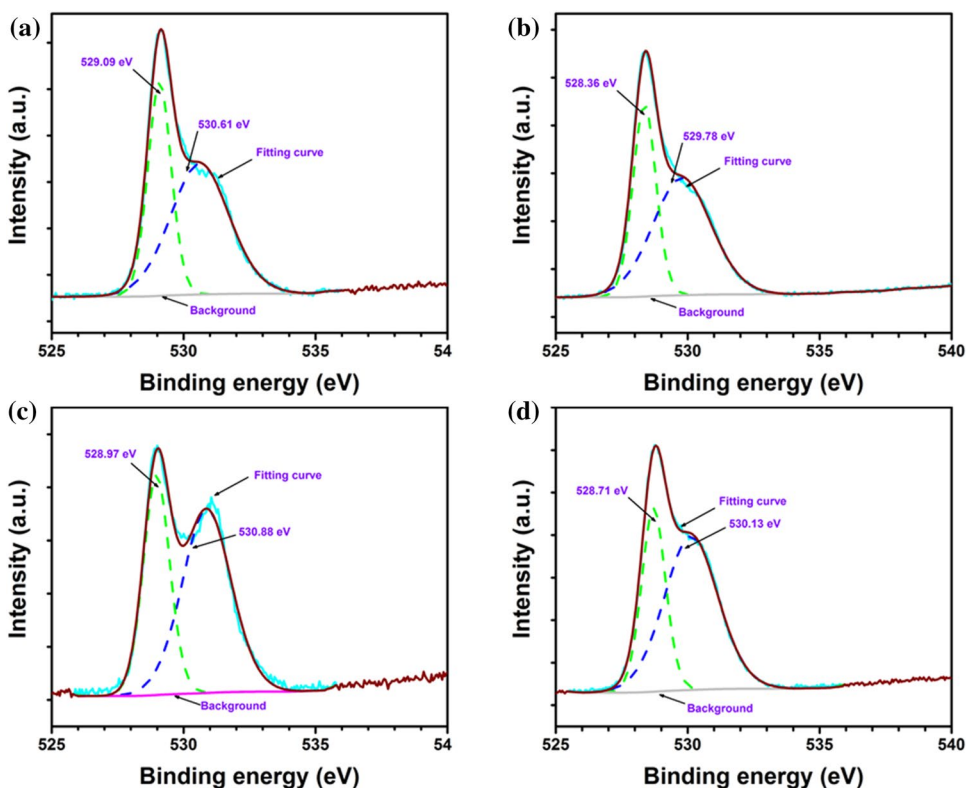
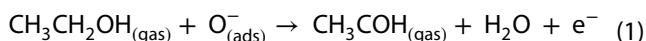


Table 3 Oxygen percentages of ITO materials with different morphologies

	Film	Particle	Nanorod	Nanowire
Adsorbed oxygen	62.21	61.24	60.82	65.34
Lattice oxygen	37.79	38.76	39.18	34.66

decreasing. The reaction can be described as the reaction Eq. 1.



The state of absorbed oxygen ion can be changed by the operating temperature. The followings show the reacting process [23].

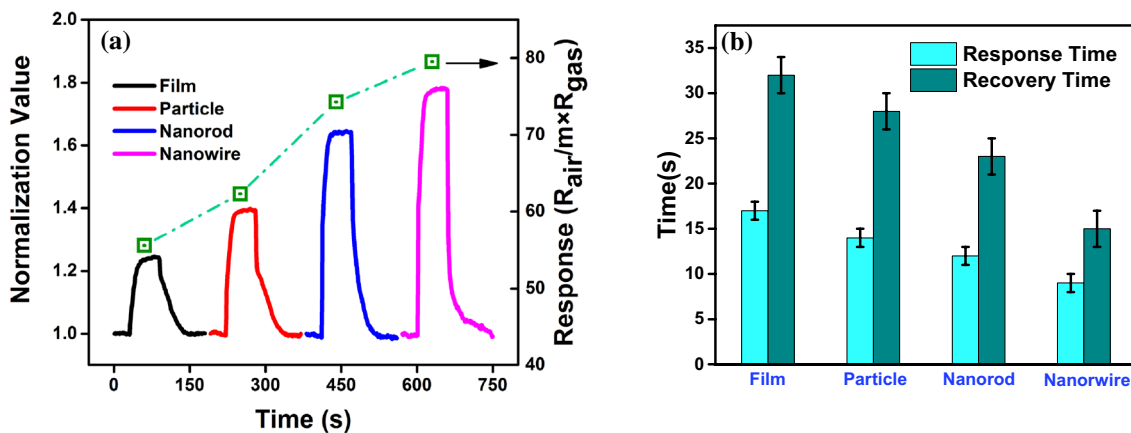
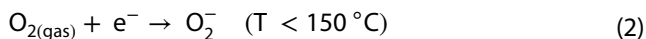
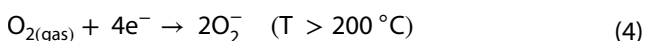
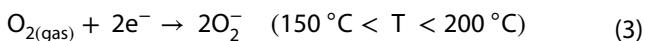
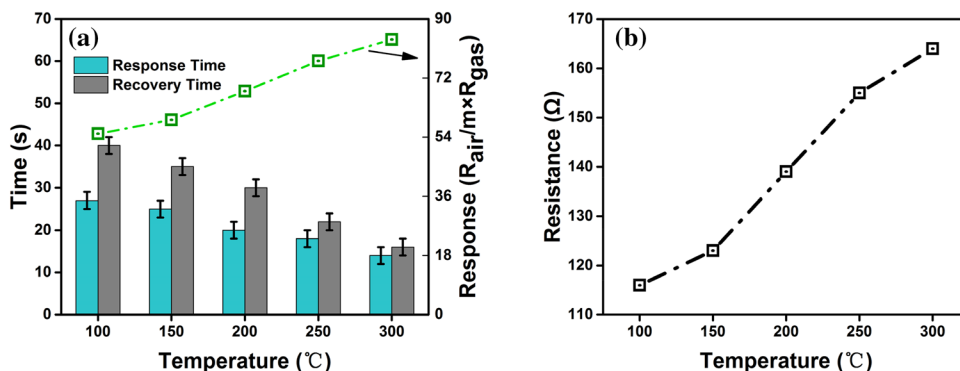


Fig. 6 a Gas sensing properties of the ITO sensors with different morphologies (film, nanoparticle, nanorod, and nanowire) at the condition of the ethanol gas concentration of 400 ppm and the

temperature of 250 °C. **b** Response and recovery time of the ITO sensors with different morphologies

Fig. 7 **a** Gas sensing properties, **b** the resistance of ITO-nanowire sensor at different operating temperatures in air



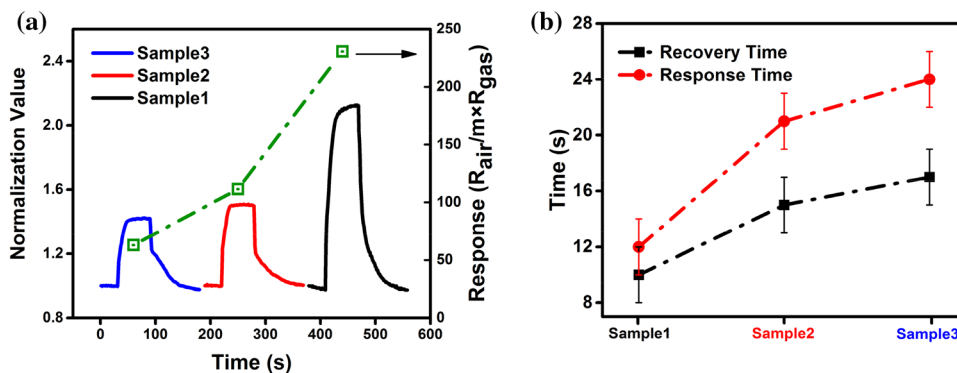
At high temperature, the oxygen vacancies could be produced, which determined the resistance of the gas sensitive materials. The more oxygen vacancies in the material, the more sensitive the sensor is. In Fig. 7a, the response and recovery time of ITO-nanowire sensor at different operating temperature was summarized. The resistances of ITO-nanowire at different temperatures were shown in Fig. 7b. At the temperatures of 100 °C, 150 °C, 200 °C, 250 °C and 300 °C, the corresponding response/recovery time are 24 s/40 s, 25 s/35 s, 20 s/30 s, 18 s/22 s, and 14 s /16 s, respectively. The response and recovery time decreased with the increasing of temperature.

Thirdly, the effect of ITO-nanowire density on the gas sensing performance was discussed. The gas sensors based on different densities of ITO nanowires have been fabricated, and the SEM images were shown in the Fig. 3. The ethanol gas concentration of 400 ppm and the working temperature of 250 °C were selected. From sample-1 to sample-3, the ITO-nanowire densities increased. In order to compare the gas sensing properties of the three morphologies more clearly, the normalization value was

used. The normalization value is the ratio of the output voltage under ethanol gas to the output voltage in air. In Fig. 8a, the RS was 235.6, 111.1, and 63.5, respectively. The response/recovery time was 10 s/12 s, 15 s/21 s and 17 s/21 s (Fig. 8b), respectively. The gas sensing properties reduced with the increasing of density. When the growth time becomes longer, the higher density of nanowires can be obtained. But most of nanowires were intertwined with each other, which made ethanol gas difficult to enter the gap between nanowires and reduced the reaction area with ITO nanowires. Choosing proper nanowire density is also an important factor for high-performance sensor.

Based on the sample-1, the output voltage of sensor was tested at different ethanol gas concentrations at the same working temperature of 250 °C. The results were presented in Fig. 9a and b. The higher the ethanol gas concentration is, the higher voltage can be obtained. The response of gas sensor was expressed by the change of voltage (the test circuit has been shown in Fig. 1), the corresponding resistance of ITO nanowires at different ethanol gas concentration could be found in appendix Fig. 12. Under the concentration of 2500 ppm, the RS reached to 287.2, and the response/recovery time reduced to 10 s/12 s. More importantly, the sensitivity is still high (196.6) even under the gas concentration of 50 ppm, showing a good gas sensing performance. This sensor

Fig. 8 **a** The sensing properties, **b** response and recovery time of ITO-nanowire sensor with different densities



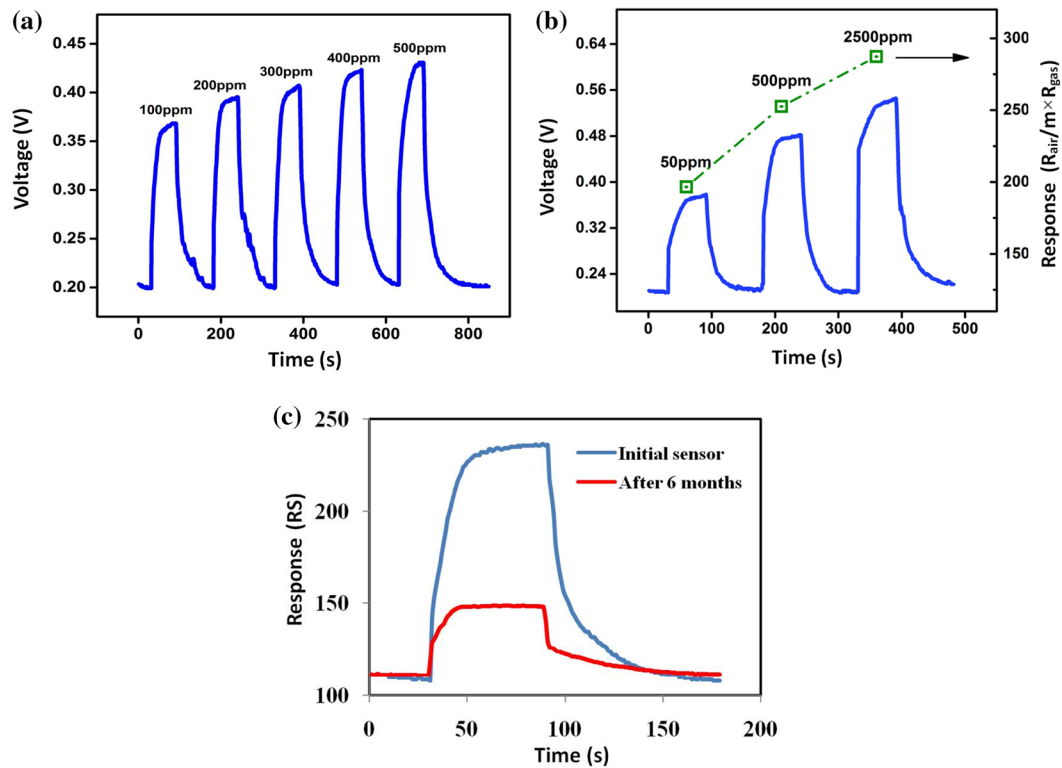


Fig. 9 The response of ITO nanowires sensor sample-1 at different ethanol gas concentrations with **a** small concentration interval and **b** large concentration interval; **c** at different test time

also shows long-term stability. Under the same conditions (400 ppm of ethanol gas concentration and the temperature of 250 °C), the response of the same gas sensor was tested after half a year. The results are shown in Fig. 9c. The response value decreased from 235 to 148 because of ITO materials' mildew effect, but the general trend remained unchanged.

3.4 Gas sensing enhancing mechanism of ITO NWs

From the above discussion, the gas response of nanowire was the best. Apart from the high specific surface area of nanowires, the content of oxygen vacancy in the material should be an important factor affecting the gas sensing properties. Based on the XPS analysis (Table 2), the Sn element is the highest in nanowire. The higher Sn content is, the more oxygen vacancies occur in the material [13]. The content of oxygen vacancy and the reaction area with ethanol gas are increasing from ITO film to nanowire (Fig. 10). When oxygen vacancies react with gas molecules, the effective electron transport channel determines the speed of the reaction. The electron transport channels in different materials were shown in Fig. 10. The transmission direction is within 360° in film, and the angle becomes smaller and smaller with the reduction of material

dimension. The direction becomes the only specific one in the nanowire, which improved the sensitivity of sensor.

3.5 First principle calculation of ITO materials with different Sn-doping concentrations

From XPS analyze result (Fig. 5 and Table 2), the Sn atomic percentage increases when the morphology changes from film to nanowire. To further explain the phenomenon that RS changes with the change of morphology, the surface adsorption energy of ITO materials with different morphologies was calculated by the first principle calculation method. Based on the conventional unit cell of indium oxide, different doping concentrations can be achieved by replacing In atoms with Sn atoms. In_2O_3 has two crystal structures: rhombohedral structure and cubic bixbyite structure, and the latter is more stable [24]. For cubic bixbyite In_2O_3 , the space group symmetry being Ia3 with the lattice constant $a = 10.117 \text{ \AA}$, the unit cell contains 80 atoms. According to Wyckoff's notation, the unit cell contains 48 oxygen atoms at e sites, 24 indium atoms at d sites, and 8 indium atoms at b sites.

Figure 11a shows the crystal structure of In_2O_3 . In_2O_3 belongs to strongly correlated electron system [25], the

Fig. 10 The reaction mechanism of different materials

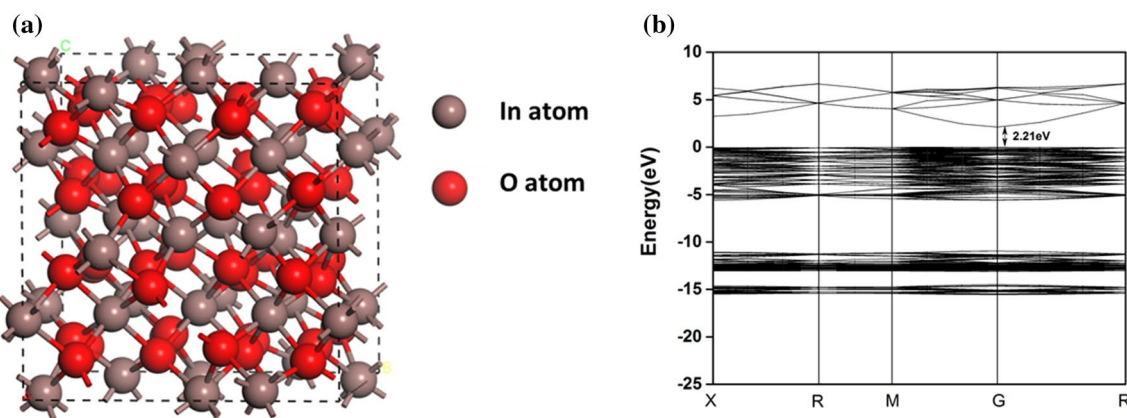
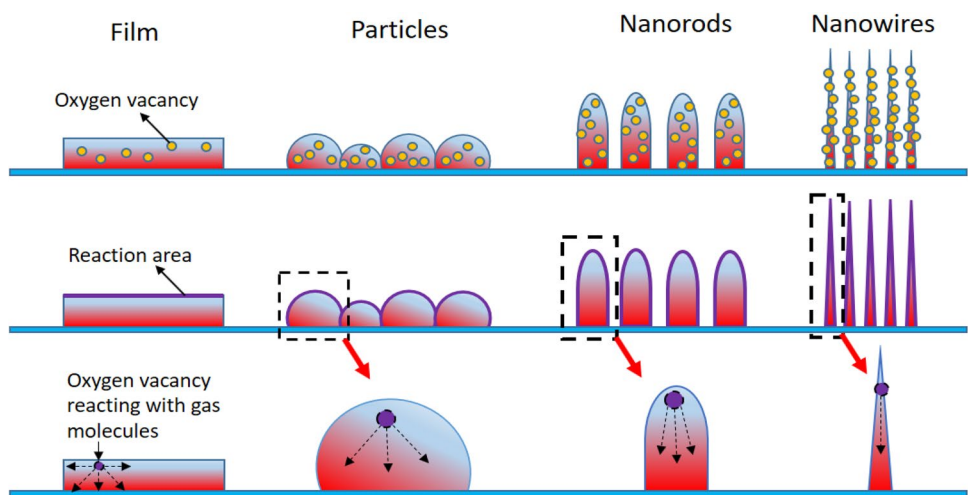


Fig. 11 a Crystal structure and b band structure of pure In_2O_3

Coulombic potentials of In-4d and O-2p should be considered. So LDA + U method was used, $U_{\text{In-4d}} = U_{\text{Sn-4d}} = 3 \text{ eV}$, and $U_{\text{O-2p}} = 5 \text{ eV}$. The energy band structure of pure indium oxide was calculated firstly to verify the correctness of the model, Fig. 11b shows that the energy band of pure In_2O_3 is 2.21 eV, which is close to reported [26]. Then, different doping concentration is achieved, and doped Sn atom number is 2, 3, 4 and 5, respectively. The appendix materials (Figs. 13, 14) show the results of first principle calculation for different doping concentration. To obtain the adsorption energy of oxygen on the different morphologies, the energy of the ITO (100) crystal plane were calculated before and after oxygen adsorption, as shown in Table 4.

The adsorption energy can be calculated by the following formula:

$$E_{\text{adsorption}} = E_{\text{ITO(100)+O}_2} - E_{\text{ITO(100)}} - E_{\text{O}_2} \text{ (The } E_{\text{O}_2} = -864.14 \text{ eV)} \quad (5)$$

Table 4 Proportion of indium and tin atoms in different morphologies

Proportion of Sn	$E_{\text{ITO(100)+O}_2}$ (eV)	$E_{\text{ITO(100)}}$ (eV)	$E_{\text{adsorption}}$ (eV)
$\text{In}_2\text{O}_3\text{-2Sn}$	-68,771.07	-67,904.72	-2.21
$\text{In}_2\text{O}_3\text{-3Sn}$	-67,305.47	-66,439.55	-1.78
$\text{In}_2\text{O}_3\text{-4Sn}$	-65,840.55	-64,975.16	-1.25
$\text{In}_2\text{O}_3\text{-5Sn}$	-64,375.52	-63,510.22	-1.16

The results show that the adsorption energy of oxygen decreases with increasing the doping concentration. ITO nanowires could absorb more oxygen ions at the same conditions, and more carriers were generated after the reaction between ethanol and oxygen ions.

4 Conclusions

The ITO materials with different morphologies were fabricated via sputtering by adjusting the RF-power and the oxygen flow rate. The gas sensors have been prepared with ceramic tube directly, and the gas sensing properties of the whole ITO material system (film, nanoparticles, nanorods and nanowires) were studied. The nanowires have larger specific surface area, more oxygen vacancies and an oriented electron transport channel, so the sensing property is the best. The sensing performance to ethanol gas has been improved significantly by controlling the density of nanowires. Under the operating temperature of 250 °C, the RS of the sensor with appropriate ITO nanowires was 235.6 at the ethanol gas concentration of 400 ppm. And, the response and recovery time is 10 s and 12 s, respectively. Finally, the oxygen adsorption energy of different morphologies was calculated by first-principle calculation method. The calculation results are consistent with experiment results, which show that the oxygen adsorption energy decreases with the morphologies changing from film to nanowire. These results provide guidance for the application of ITO materials in the field of gas sensors.

Acknowledgements This work was supported by the grant from the National Key R&D Program of China (No. 2016YFB0400801), the Natural Science Foundation of Shaanxi Province (No. 2017JQ6013) and the China Postdoctoral Science Foundation (No. 2014M562415), and the Fundamental Research Funds for the Central Universities (No. xjj2017011).

Compliance with ethical standards

Conflict of interest On behalf of all authors, the corresponding author states that there is no conflict of interest.

Appendix

See Figs. 12, 13, 14.

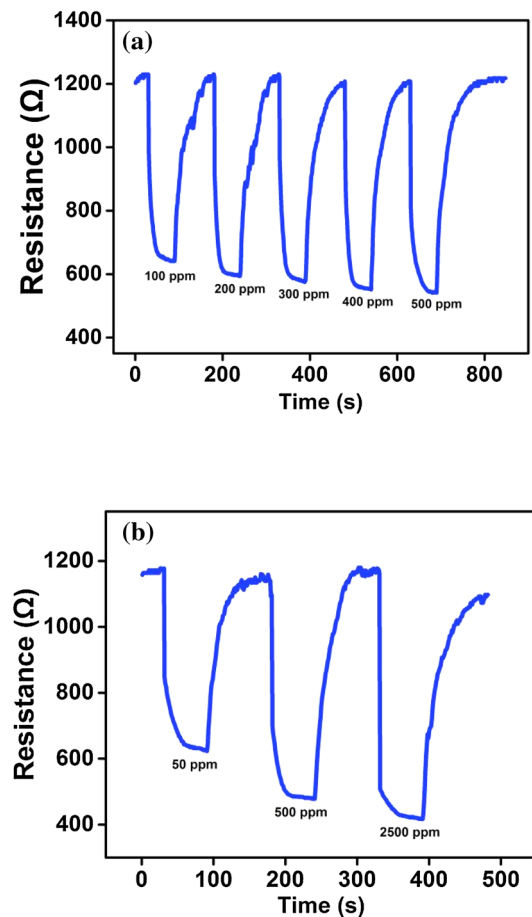


Fig. 12 The sensitivity of ITO nanowires sensor sample1 at different ethanol gas concentrations

Fig. 13 The crystal structure of ITO materials with different Sn-doping concentration **a** $\text{In}_2\text{O}_3\text{-2Sn}$, **b** $\text{In}_2\text{O}_3\text{-3Sn}$, **c** $\text{In}_2\text{O}_3\text{-4Sn}$, **d** $\text{In}_2\text{O}_3\text{-5Sn}$

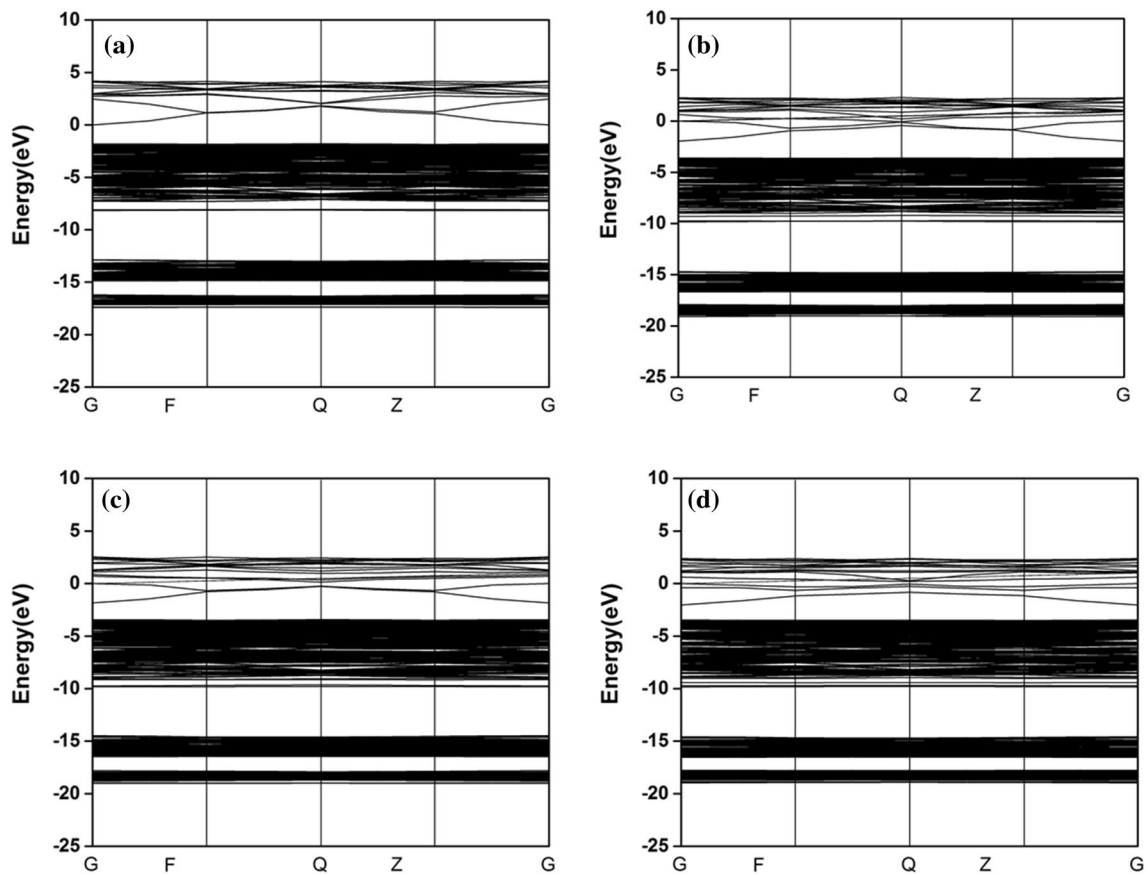
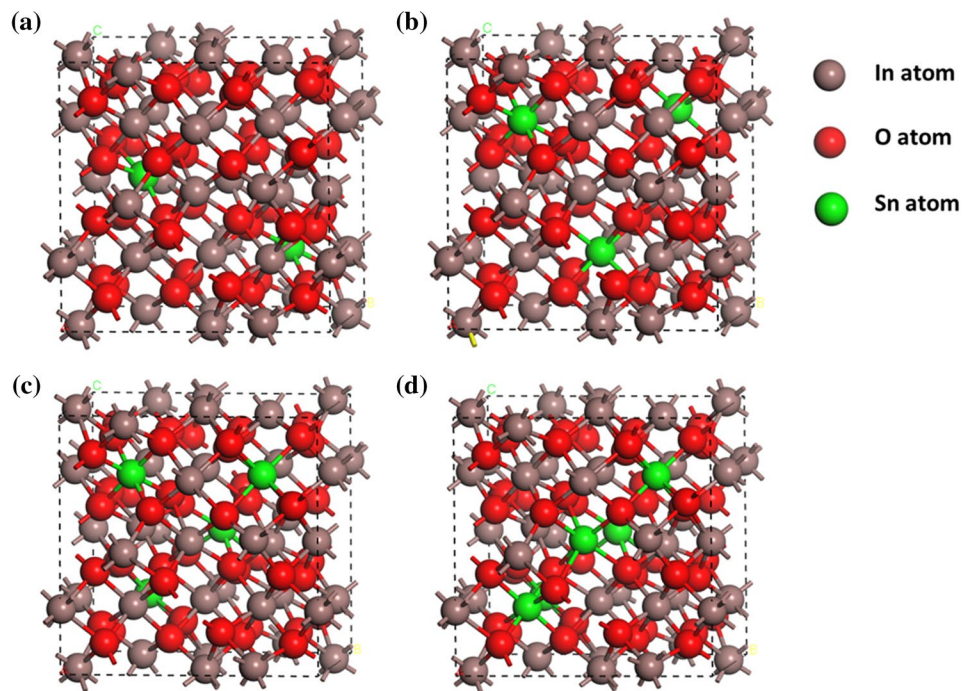


Fig. 14 The band structure of ITO materials with different Sn-doping concentration **a** $\text{In}_2\text{O}_3\text{-2Sn}$, **b** $\text{In}_2\text{O}_3\text{-3Sn}$, **c** $\text{In}_2\text{O}_3\text{-4Sn}$, **d** $\text{In}_2\text{O}_3\text{-5Sn}$

References

1. Lin CW, Chen HI, Chen TY, Huang CC, Hsu CS, Liu RC, Liu WC (2011) On an indium–tin-oxide thin film based ammonia gas sensor. *Sens Actuators B* 160:1481–1484
2. Yoo KS, Park SH, Kang JH (2005) Nano-grained thin-film indium tin oxide gas sensors for H₂ detection. *Sens Actuators B* 108:159–164
3. Kim H, Kumar MD, Patel M, Kim J (2016) ITO nanowires-embedding transparent NiO/ZnO photodetector. *Mater Res Bull* 83:35–40
4. Nguyen P, Ng HT, Kong J, Cassell AM, Quinn R, Li J, Meyyappan M (2003) Epitaxial directional growth of indium-doped tin oxide nanowire arrays. *Nano Lett* 3:925–928
5. Nuchuay P, Chaikereee T, Horprathum M, Mungkung N, Kasayapanand N, Oros C, Muthitamongkol P (2017) Engineered omnidirectional antireflection ITO nanorod films with super hydrophobic surface via glancing-angle ion-assisted electron-beam evaporation deposition. *Curr Appl Phys* 17:222–229
6. Lin D, Wu H, Zhang R, Pan W (2007) Preparation and electrical properties of electro spun tin-doped indium oxide nanowires. *Nanotechnology* 18:465301
7. O'Dwyer C, Szachowicz M, Visimberga G, Lavayen V, Newcomb SB, Torres CS (2009) Bottom-up growth of fully transparent contact layers of indium tin oxide nanowires for light-emitting devices. *Nat Nanotechnol* 4:239
8. Vaishnav VS, Patel PD, Patel NG (2005) Preparation and characterization of indium tin oxide thin films for their application as gas sensors. *Thin Solid Films* 487:277–282
9. Jiao Z, Wu M, Gu J, Sun X (2003) The gas sensing characteristics of ITO thin film prepared by sol–gel method. *Sens Actuators B* 94:216–221
10. Ayeshamariam A (2013) Size-controllable synthesis of ITO nanoparticles and application in gas sensor devices. *J Photonics Spintron* 2:4–7
11. Yao K, Toole R, Basnet P, Zhao Y (2014) Highly sensitive double-layered nanorod array gas sensors prepared by oblique angle deposition. *Appl Phys Lett* 104:622–659
12. Afshar M, Preiß EM, Sauerwald T, Rodner M, Feili D, Straub M (2015) Indium-tin-oxide single-nanowire gas sensor fabricated via laser writing and subsequent etching. *Sens Actuators B* 215:525–535
13. Zhou JY, Bai JL, Zhao H, Yang ZY, Gu XY, Huang BY (2018) Gas sensing enhancing mechanism via doping-induced oxygen vacancies for gas sensors based on indium tin oxide nanotubes. *Sens Actuators B* 265:273–284
14. Noh JH, Han HS, Lee S, Kim JY, Hong KS, Han GS, Jung HS (2011) Nanowire-based three-dimensional transparent conducting oxide electrodes for extremely fast charge collection. *Adv Energy Mater* 1:829–835
15. Fung MK, Sun YC, Ng AMC, Chen XY, Wong KK, Djurišić AB, Chan WK (2011) Indium tin oxide nanowires growth by dc sputtering. *Appl Phys A* 104:1075–1080
16. Pokaipisit A, Udomkan N, Limsuwan P (2006) Nanostructure and properties of indium tin oxide (ITO) films produced by electron beam evaporation. *Mod Phys Lett B* 20:1049–1058
17. Yamamoto N, Morisawa K, Murakami J, Nakatani Y (2014) Formation of ITO nanowires using conventional magnetron sputtering. *ECS Solid State Lett* 3:84–86
18. Shigesato Y, Paine DC (1994) A microstructural study of low resistivity tin-doped indium oxide prepared by dc magnetron sputtering. *Thin Solid Films* 238:44–50
19. Li Q, Zhang Y, Feng L, Wang Z, Wang T, Yun F (2018) Investigation of growth parameters influence on self-catalyzed ITO nanowires by high RF-power sputtering. *Nanotechnology* 29:165708
20. Pillay VV, Goyal S (2015) Influence of sputtering power, annealing on the structural properties of ITO films, for application in ethanol gas sensor. *Mater Today Proc* 2:4609–4619
21. Wang C, Yin L, Zhang L, Xiang D, Gao R (2010) Metal oxide gas sensors: sensitivity and influencing factors. *Sensors* 10:2088–2106
22. Liu X, Cheng S, Liu H, Hu S, Zhang D, Ning H (2012) A survey on gas sensing technology. *Sensors* 12:9635–9665
23. Yang Z, Huang Y, Chen G, Guo Z, Cheng S, Huang S (2009) Ethanol gas sensor based on Al-doped ZnO nanomaterial with many gas diffusing channels. *Sens Actuators B* 140:549–556
24. Bai LN, Wei YP, Lian JS, Jiang Q (2013) Stability of indium–tin-oxide and its optical properties: a first-principles study. *J Phys Chem Solids* 74:446–451
25. Gurlo A, Ivanovskaya M, Barsan N, Weimar U (2003) Corundum-type indium(III) oxide: formation under ambient conditions in Fe₂O₃–In₂O₃ system. *Inorg Chem Commun* 6:569–572
26. Lin XL, Chen ZP, Gao H, Pan FC, Wang XM, Chen HM (2016) The electronic structures and magnetic properties of un-doped In₂O₃: the first-principle calculation. *J Supercond Nov Magn* 29:1533–1537

Publisher's Note Springer Nature remains neutral with regard to jurisdictional claims in published maps and institutional affiliations.